Supplementary Material

Results and Discussion

Conformational changes in the chaperone–subunit complex upon binding to $FimD_N$

The structures of FimC and $FimH_P$ in the ternary complex are overall closely similar to those in the previously published binary complex (PDB entries 1QUN and 1KIU) (Choudhury *et al*, 1999; Hung *et al*, 2002). The r.m.s.d. value is 1.3 Å for the 318 common C^{α} atoms (chains A and B from PDB entry 1QUN were used for the comparison). In a region where electron density was unambiguous in our structure of the ternary complex, we observed a register shift involving 5 residues in the A strand of $FimH_P$ (residues 169–173), which are in direct contact with the donor strand G_1 of FimC. Using the structure factors available for the PDB entry 1KIU, we recalculated an electron density map for the ternary complex after simulated annealing at 5000 K and B-factor refinement. The revised density and a bioinformatic analysis (M. Sippl, personal communication) lead to a model that, in contrast to 1QUN and 1KIU, does not exhibit a register shift with respect to the ternary complex. After taking this into account, significant conformational changes can still be observed near the binding site of the donor strand. Specifically, the $FimD_N$ arm of residues 1–24 pushes Met93 of FimC towards FimH upon binding, in order to accommodate Tyr3 of $FimD_N$. This leads to a twisting of the segment of residues 92–100 of FimC, which precedes the donor strand, and the flexible loop 213–217 of $FimH_P$ is pushed away. The rotation of FimC Met93 also causes additional rearrangements in $FimH_P$. These include that through a contact with the $C^{\gamma 2}$ atom of $FimH_P$ Thr169, the FimC Met93 side chain forces the residues 165–170 of $FimH_P$ to adopt a different conformation. As a consequence, the side chain of $FimH_P$ Val168, which is solvent-

exposed in the binary complex, is pushed into a hydrophobic groove formed by Tyr31, Pro91, Leu105, Ile107 of FimC and Ala165 of $FimH_P$ (Supplementary Figure S4).

Materials and methods

X-ray structure determination of the $FimD_N(1–125)$–FimC–$FimH_P$ ternary complex

Crystals were cryo-protected either by stepwise addition of 2-methyl-2,4-pentanediol to a final concentration of 20% (form A), or of ethylene glycol to 20% (form B). Data were collected at 100 K using synchrotron radiation (beamline X06SA at the Swiss Light Source) and processed with DENZO (Otwinowski and Minor, 1996) and with programs of the CCP4 suite (Collaborative Computational Project, 1994). The structure of the ternary complex was solved by molecular replacement with AMoRe (Navaza, 1994), using the data from crystal form A. The search model was a truncated version of the binary FimC–FimH complex [(Choudhury *et al*, 1999), PDB entry 1QUN] in which the FimH lectin domain had been deleted. Additional electron density for $FimD_N(1–125)$ appeared already with the initial molecular replacement phases. Several cycles of model building with O (Jones *et al*, 1991) and structure refinement with CNS (Brunger *et al*, 1998) yielded a nearly complete model of $FimD_N(1–125)$ and improved density for the other two proteins. The model of the ternary complex obtained in this way was used for straightforward molecular replacement with AMoRe against the 1.84 Å orthorhombic data. Refinement was carried out with CNS, using a bulk solvent correction and applying no sigma cut-off. Water molecules were added at positions where clear electron density was seen in Fo-Fc maps and where the environment allowed reasonable hydrogen bonding to the protein or to other water molecules. Structure validation was performed with the programs PROCHECK (Laskowski *et al*, 1993) and WHAT_CHECK (Hooft *et al*, 1997).

Characterization of FimC and FimD variants

To analyze the expression of FimD variants in the outer membrane, W3110Δ*fimD* encoding wild-type *fimD* or *fimD* variants were grown in M9 minimal medium without shaking. After two days, cells were harvested, resuspended in 20 mM Tris/HCl (pH 8.0), and lysed by sonication. After unbroken cells were removed by centrifugation, Sarkosyl (N-lauroylsarcosine sodium salt) was added to the supernatant to a final concentration of 0.5%, and the mixture was rocked for 20 min at 25 ºC to selectively solubilize the inner membrane (Nikaido, 1994). The outer membrane was then pelleted by centrifugation and resuspended in 20 mM sodium phosphate (pH 7.4), 115 mM NaCl. Immunoblot analysis was performed with anti-Penta·His antibodies (Qiagen), and an alkaline phophatase-conjugated secondary antibody (Pierce).

To analyze the expression of FimC variants in the periplasm, W3110Δ*fimC* harboring plasmid-encoded wild-type *fimC* or *fimC* variants were grown for two days in M9 minimal medium without shaking. Periplasmic extracts and immunoblot analysis with anti-FimC antibodies were performed as described previously (Nishiyama *et al*, 2003).

Isothermal titration calorimetry was carried out as described previously (Nishiyama *et al*, 2003). Thermal unfolding of truncated $FimD_N$ variants was measured by far-UV CD at 218 nm with a protein concentration of 10 μM in 20 mM sodium phosphate (pH 7.4), 115 mM NaCl. The experimental data were analyzed according to the two-state model of folding, using a six-parameter fit (Pace *et al*, 1998). Electron micrographs of *E. coli fimD* deletion strains complemented with plasmids encoding different FimD variants were recorded as described previously (Nishiyama *et al*, 2003).

Table S I: Thermal unfolding of truncated $FimD_N$ variants at pH 7.4.

$FimD_N$ variants	$FimD_N$(25−139)	$FimD_N$(1−125)	$FimD_N$(1−139)
T_m (K)	340.4 ± 0.4	340.3 ± 0.4	341.1 ± 0.4

Table S II: Thermodynamic parameters obtained from calorimetric titrations of various $FimD_N$ variants with the FimC−$FimH_P$ complex at pH 7.4 and 25 °C. The *n*-value denotes the binding stoichiometry calculated from the calorimetric data.

$FimD_N$ variants	*n*-value	K_D (10^{-6} M)	ΔH (kJ mol^{-1})	ΔG (kJ mol^{-1})	ΔS (J mol^{-1} K^{-1})
$FimD_N$ (1−139; D36A)	1.14 ± 0.02	7.09 ± 0.48	–42.6 ± 1.2	–29.4 ± 0.2	−44.3
$FimD_N$ (1−139; Q109A)	1.02 ± 0.01	4.15 ± 0.17	–49.5 ± 0.6	–30.7 ± 0.2	−62.9
$FimD_N$ (1−139; WT)	0.88 ± 0.01	1.23 ± 0.07	–50.2 ± 1.2	–33.7 ± 0.1	−57.0
$FimD_N$ (1−125; WT)	0.98 ± 0.01	1.14 ± 0.01	–52.9 ± 1.2	–33.9 ± 0.1	−63.4

References for supplementary information

Brunger, A.T., Adams, P.D., Clore, G.M., DeLano, W.L., Gros, P., Grosse-Kunstleve, R.W., Jiang, J.S., Kuszewski, J., Nilges, M., Pannu, N.S., Read, R.J., Rice, L.M., Simonson, T. and Warren, G.L. (1998) Crystallography & NMR system: A new software suite for macromolecular structure determination. *Acta Crystallogr D Biol Crystallogr*, **54**, 905-921.

Choudhury, D., Thompson, A., Stojanoff, V., Langermann, S., Pinkner, J., Hultgren, S.J. and Knight, S.D. (1999) X-ray structure of the FimC-FimH chaperone-adhesin complex from uropathogenic Escherichia coli. *Science*, Vol. 285, pp. 1061-1066.

Collaborative Computational Project, N. (1994) The CCP4 suite: programs for protein crystallography. *Acta Crystallogr D Biol Crystallogr*, **50**, 760-763.

Hooft, R.W., Vriend, G., Sander, C. and Abola, E.E. (1997) Errors in protein structures. *Nature*, **381**, 272.

Jones, T.A., Zou, J.Y., Cowan, S.W. and Kjeldgaard. (1991) Improved methods for building protein models in electron density maps and the location of errors in these models. *Acta Crystallogr A*, **47 (Pt 2)**, 110-119.

Laskowski, R.A., MacArthur, M.W., Moss, D.S. and Thornton, J.M. (1993) PROCHECK: a program to check the stereochemical quality of protein structure. *J. Appl. Cryst.*, **26**, 283-291.

Navaza, J. (1994) *AMoRe*: an automated package for molecular replacement. *Acta Cryst.*, **A50**, 157.

Nishiyama, M., Vetsch, M., Puorger, C., Jelesarov, I. and Glockshuber, R. (2003) Identification and characterization of the chaperone-subunit complex-binding domain from the type 1 pilus assembly platform FimD. *J Mol Biol*, Vol. 330, pp. 513-525.

Otwinowski, Z. and Minor, W. (eds.). (1996) *Processing of X-ray diffraction data collected in oscillation mode*. Academic Press.

Pace, C.N., Hebert, E.J., Shaw, K.L., Schell, D., Both, V., Krajcikova, D., Sevcik, J., Wilson, K.S., Dauter, Z., Hartley, R.W. and Grimsley, G.R. (1998) Conformational stability and thermodynamics of folding of ribonucleases Sa, Sa2 and Sa3. *J Mol Biol*, Vol. 279, pp. 271-286.

Figure legends

Figure S1: Heteronuclear [^{15}N,^{1}H]-NOEs of free $FimD_N$(1−139). Values between 0.5 and 1 indicate well-structured parts of the protein, values < 0.5 manifest increased flexibility.

Figure S2: (A) C^{α}-Superposition of the $FimD_N$(25−139) NMR solution structure on the crystal structure of the ternary complex. Both models are shown in C^{α}-trace representation. The NMR model is depicted in red, and $FimD_N$ bound to FimC and FimH in the crystal structure is depicted in green. Residues 126−139 of $FimD_N$ (present only in the NMR structure) are depicted in blue. The NMR conformer with the smallest r.m.s.d. to the mean coordinates of the bundle of 20 DYANA conformers was chosen for the superposition. A r.m.s.d. of 1.19 Å was calculated for the C^{α}-atoms of the 94 aligned residues 28−121 of FimD. The right panel shows the same superposition as in the left panel, rotated by ~ 90 º around the vertical axis. (B) Close-up view of the C-terminal hinge segment of $FimD_N$. (C) Stereo close-up view of the $FimD_N$ region around Arg47. The NMR solution structures of $FimD_N$(25−139) (blue) and $FimD_N$(25−125) (red) are shown in backbone mode and superimposed on the crystallographic ternary complex (green). Arg47, Asp48 and residues 130, 133 and 135 of $FimD_N$ are shown in stick mode. Residues from the C-terminus of $FimD_N$ that would clash with Arg47 in the conformation observed in the X-ray structure or in the NMR structure of $FimD_N$(25−125) are labeled.

Figure S3: (A) Electron micrographic studies on *E. coli* strains W3110Δ*fimD* complemented with plasmids encoding FimD variants $FimD_{F4A}$, $FimD_{F8A}$ and wild-type FimD. The arrows show type 1 pili. (B) Expression of FimD variants in the outer membrane (OM). OMs were isolated from strain W3110Δ*fimD* cells used to express the indicated FimD variants. Samples

were incubated for 5 min at 95 ºC in SDS sample buffer prior to electrophoresis. FimD was detected by immunoblotting with the anti-Penta·His antibodies (Qiagen). (C) Expression of FimC variants in the periplasm. Periplasmic extracts were prepared from strain W3110Δ*fimC* cells used to express the indicated FimC variants. FimC was detected with the anti-FimC antibodies.

Figure S4: Stereo view of the conformational changes taking place in $FimH_P$ and FimC upon binding of $FimD_N$ to the binary complex. The structure of the ternary complex ($FimD_N$ in green, FimC in cyan and $FimH_P$ in yellow) is superimposed onto that of the binary complex (both FimC and FimH in magenta; see Results and Discussion for details). Black arrows indicate the displacements caused by the binding of $FimD_N$ (especially Tyr3): FimC Met93, $FimH_P$ Thr169 and Val168 are displaced and Val168 is pushed into a hydrophobic groove formed by Tyr31, Pro91, Leu105 and Ile107 of FimC and by Ala165 of $FimH_P$.

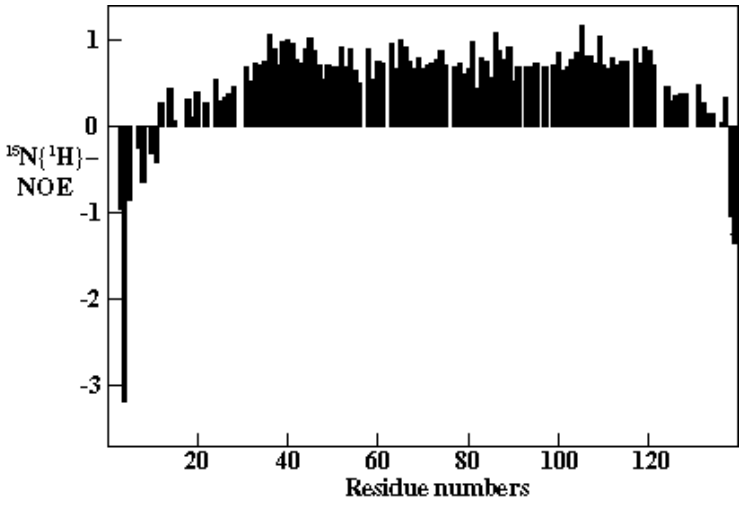
1
0
-1
-2
-3
15N{1H}–
NOE
20
40
60
80
100
120
Residue numbers

A

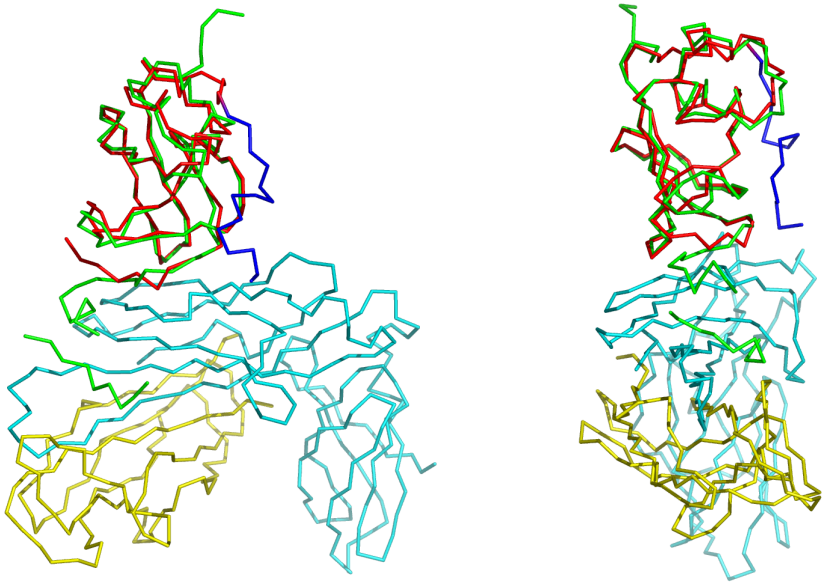

B

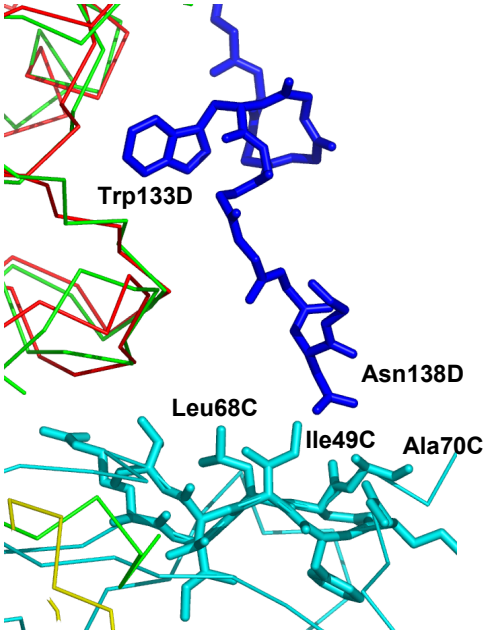
Trp133D
Asn138D
Leu68C
Ile49C
Ala70C

C

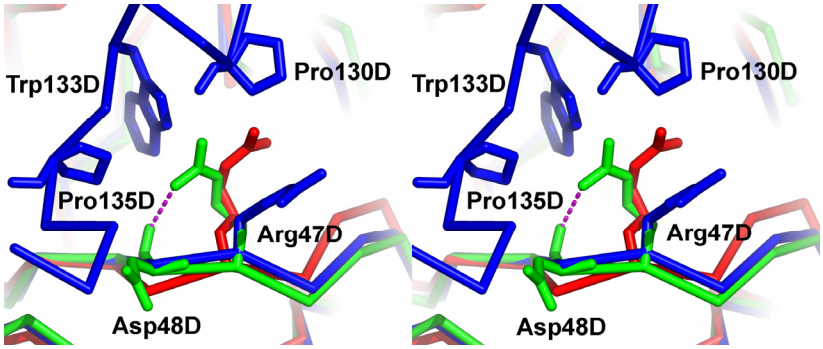
Trp133D
Pro130D
Pro135D
Arg47D
Asp48D
Trp133D
Pro130D
Pro135D
Arg47D
Asp48D

A

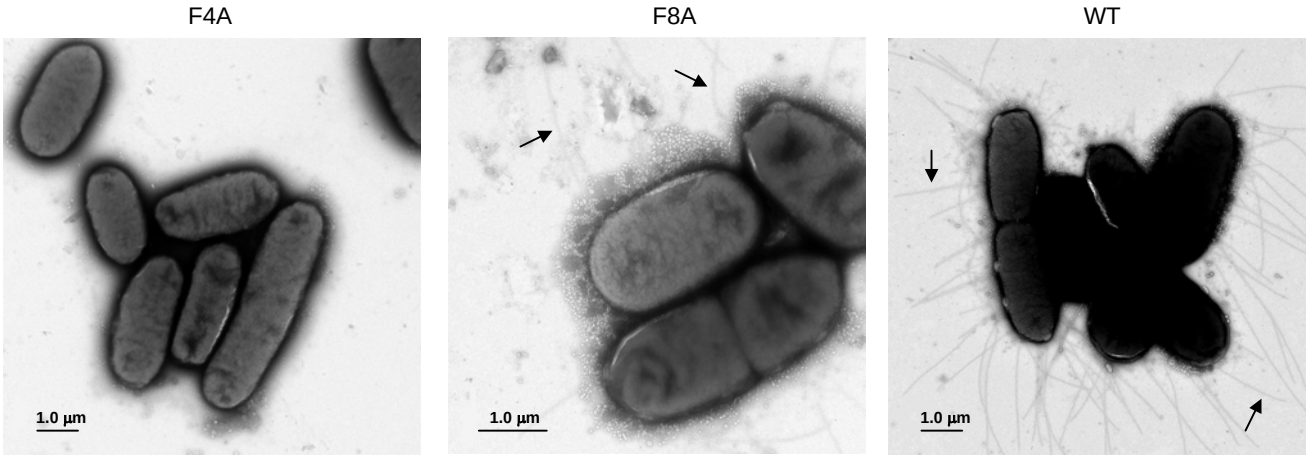
F4A
F8A
WT
1.0 µm
1.0 µm
1.0 µm

B

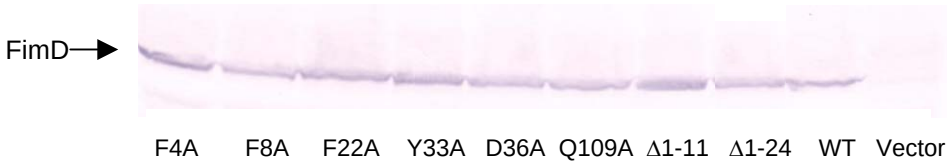
FimD
F4A
F8A
F22A
Y33A
D36A
Q109A
Δ1-11
Δ1-24
WT
Vector

C

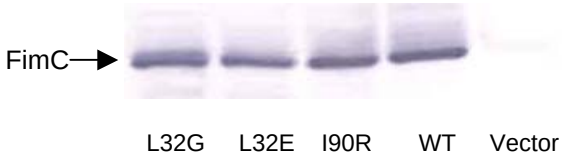
FimC
L32G
L32E
I90R
WT
Vector

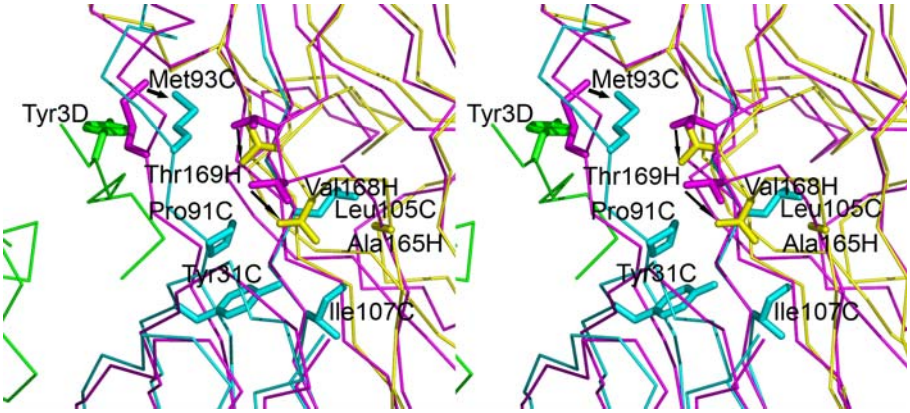
Met93C
Tyr3D
Thr169H
Val168H
Pro91C
Leu105C
Ala165H
Tyr31C
Ile107C
Met93C
Tyr3D
Thr169H
Val168H
Pro91C
Leu105C
Ala165H
Tyr31C
Ile107C